Journal of Advanced Joining Processes 10 (2024) 100270

Contents lists available at ScienceDirect

Journal of Advanced Joining Processes

journal homepage: www.sciencedirect.com/journal/journal-of-advanced-joining-processes

Ablation treatment of CFRP via nanosecond pulsed Ytterbium-doped fiber laser: Effects of process parameters on surface morphology and shear strength of adhesive bonded joints

Chiara Mandolfino [a,*], Fabrizio Moroni [b], Marco Pizzorni [a]

[a] Department of Mechanical, Energy, Management and Transport Engineering, Polytechnic School, University of Genoa, Via All'Opera Pia 15, 16145, Genoa, Italy
[b] Dipartimento di Ingegneria dei Sistemi e delle Tecnologie Industriali – DISTI, Università di Parma, Parco Area Delle Scienze 181/A, 43124, Parma, Italy

ARTICLE INFO

Keywords:
Fiber laser treatment
Adhesive bonding
Ablation rate
CFRP

ABSTRACT

Adhesive bonding is the joining technique that provides the maximum exploitation of Carbon Fiber Reinforced Polymers (CFRPs) for structural applications. However, it is necessary to attain a high-strength adhesive bond, achieved by removing surface contaminants, such as mold release agents, and simultaneously generating a surface structure suitable to increase the actual contact surface area. The purpose of the research work presented in this paper is to evaluate the effect of process parameters of a nanosecond pulsed laser pre-bonding surface treatment on the ablation of thermoset matrix CFRP substrates. In particular, the link between the volume of ablated material and the tensile shear strength (TSS) of adhesive bonded joints was evaluated by lap-shear tests, profilometer surveys, and Scanning Electron Microscope (SEM) analysis. ANOVA and regression models were used to highlight the influence of laser parameters, with power emerging as the most significant factor, and energy density proving pivotal for joint strength. Line spacing was also significant, while scanning direction had negligible impact. The key outcomes of the study demonstrated that controlled laser ablation plays a critical role in determining joint performance. A negative correlation was found between TSS and the thickness of ablated material, indicating that excessive ablation weakens the bond. Optimal joint strength was achieved with moderate fiber exposure while maintaining matrix integrity, emphasizing the need for precise control over laser parameters. Fracture surface analyses revealed distinct failure mechanisms, ranging from cohesive failure within the adhesive layer to interfacial failure at the fiber-matrix boundary, depending on the ablation conditions. The findings provide clear guidelines for optimizing laser surface treatments to enhance the structural performance of CFRP adhesive joints in practical applications.

Introduction

Adhesive-substrate interfaces play a key role in structural bonding of composites, remarkably affecting the final quality of joints. Indeed, as-they-are surfaces are often contaminated by chemical and physical agents or other residuals of the adherends' manufacturing process. This situation may prevent good adhesion conditions from being achieved, severely compromising joint reliability and durability. Consequently, pre-bonding wiping of the adherend surfaces is certainly a prerequisite for bonding. However, a clean surface is often not sufficient for structural composite joints, for which further treatments are typically needed to complete the removal of contaminants or any excess matrix, and eventually provide activation and/or texturing of the faying surface. Especially with low-surface-energy materials like polymers or polymer-matrix composites, treatment is required to stimulate the creation of functional groups at the substrate-side interface that can chemically interact with the adhesive, and/or to modify surface topography and roughness in order to promote a mechanical interconnection with the polymerized adhesive (Molitor et al., 2001; Bénard et al., 2007).

Over the years, a wide variety of treatment processes have been used industrially on composites, with varying degrees of success. Among them, mechanical treatments are commonly used in some applications due to their simplicity and affordability. Relying on increasing the surface roughness of adherends, they enable an increase in contact area and wettability, promoting the "interlocking" mechanism (del Real et al., 2011; Schweizer et al., 2017). Typical pre-bonding methods within this

* Corresponding author at: Via All'Opera Pia 15, 16145 Genoa, Italy.
E-mail address: chiara.mandolfino@unige.it (C. Mandolfino).

https://doi.org/10.1016/j.jajp.2024.100270

Available online 26 November 2024
2666-3309/© 2024 The Authors. Published by Elsevier B.V. This is an open access article under the CC BY license (http://creativecommons.org/licenses/by/4.0/).

category are those based on surface abrasion, like conventional sanding or sandblasting, and the peel-ply method (Ramaswamy et al., 2020; Kanerva and Saarela, 2013). Abrasive methods are fairly easy to perform, but difficult to reproduce as they are operator-dependent and lead to further contamination of the workpiece surface (e.g., dust) requiring additional cleaning, all of which contribute to increased cost and production time. It should be added that both processes are suitable for small parts, but unsuitable for large parts because they are difficult to automate; rather, these are typically manual processes that may increase risks damaging the fibers or, conversely, may not completely remove contamination. The morphology obtained may be uneven and difficult to control: inadequate management of the process can lead to an excessively rough surface, to the point that it is very easy for liquids or corrosive agents to penetrate and compromise the integrity of the substrate/joint (Rudawska and Jacniacka, 2009; Gomes et al., 2008; Prolongo and Ureña, 2009).

Peel-ply, on the other hand, is a mechanical method in which a thermoplastic release fabric is applied to the composite surface, prior to matrix polymerization, and removed just before bonding. After peeling off, it leaves the imprint of its weave on the surface, giving it a uniform and repeatable profile. However, it may happen that small residues of the ply remain entrapped in the matrix, affecting adhesion negatively. Indeed, peel-ply is made of low-surface-energy polymers and is often coated with release agents, which are detrimental to bonding (Kanerva and Saarela, 2013).

As an alternative treatment, laser processes are a greener, contactless, and easily automatable option that can guarantee the desired level of interaction with the material, and thus adequate cleaning and activation of the surface, as long as the process parameters are carefully chosen (Favi et al., 2021).

Over the past three decades, laser technology has been widely studied because it overcomes the drawbacks presented by other types of treatment. It is easily adaptable to all substrates, whether metallic, polymeric, or composites, due to the possibility of concentrating high levels of energy that, combined with the high speed of the process, result in minimal interaction time with the material treated. Certainly, surface preparation by laser is not always cheaper than mechanical abrasion or chemical etching but can easily be automated and integrated into the production process, showing to be suitable for the treatment of larger surfaces. Moreover, it does not require any lubricant or coolant fluids, nor additional removal of impurities.

Laser ablation is a process of controlled and localized removal of material from the surface, which occurs only when a certain threshold of energy density is overcome. Laser sources used for surface treatment enable selective removal of the most suitable amount of matrix resin without damaging the fibers. This results in an effective removal of any contaminants, such as release agents used during the manufacturing process, and in creating optimal interactions at the molecular level between the adherend and the adhesive, ensuring good bond strength (Moroni et al., 2018; Tao et al., 2018; Mandolfino et al., 2021; Bora et al., 2019). Depending on the wavelength of the laser beam, photochemical ablation can occur, that is, the energy of individual photons is high enough to break the molecular bonds of the polymer, causing the treated surface to be more reactive. The phenomenon of ablation in polymers is described by photochemical or photothermal models, which are well known and extensively reviewed in the literature (Ravi-Kumar et al., 2019; Moreno et al., 2006). Several studies show a great variability of results as the available laser sources and the type of material treated vary. Regarding composite materials, the issue of the link between the volume of matrix ablated from the composite material and the mechanical strength of bonded joints remains open.

In this study, the effect of process parameters of a nanosecond pulsed laser pre-bonding surface treatment on the ablation of thermoset matrix CFRP was investigated through an extensive experimental activity aimed at achieving optimal ablation with the minimum fiber damage possible. In particular, the trend of correlation occurring between ablated material and tensile shear strength of adhesive bonded joints was evaluated by profilometer surveys, lap-shear tests, and SEM analysis. A comparison with conventionally treated joints was also illustrated.

Materials and methods

Substrate material

Carbon Fiber Reinforced Polymer (CFRP) panels of size 350 mm × 350 mm were fabricated by hand lay-up technique by overlaying 7 carbon fiber plies with a 2/2 twill weave oriented at 0° and pre-impregnated with epoxy resin (HEXCEL® HexPly® M79). These were then cured in an autoclave for 2 h at 135 °C and pressure of 6 bar, resulting in panels of 1.50 ± 0.02 mm in thickness and Young's modulus $E = 70 \pm 5$ GPa. All substrates were extracted from said CFRP panels by waterjet cutting.

Adhesive bonding and mechanical testing

To evaluate the influence of the laser treatment parameters on the tensile shear strength (TSS) of composite bonded joints, mechanical tests were performed according to ASTM D 5868 (ASTM International n.d.) adopting joints with a single-lap configuration. Joint geometry and nominal dimensions are shown in Fig. 1.

The single lap joints (SLJs) were fabricated immediately after the surface treatment. Alignment between the two adherends, overlap length (12.5 mm), and adhesive thickness (0.05 mm) were ensured using a specifically designed jig. A two-component epoxy adhesive, 3M™ DP490 (DP490 Data Sheet), was applied and then cured according to a cycle of 24 h at 23°C followed by 1 h at 80°C, as indicated in the product's data sheet.

Two standard pre-bonding preparation procedures were performed to realize two sets of SLJs, employed as the reference joints (RJs) against which to evaluate the performance of SLJs after laser treatment; specifically: (i) simple surface cleaning with acetone solvent, and (ii) a sequence consisting of a preliminary cleaning with acetone solvent followed by manual abrasion using a 3M™ Scotch-Brite™ MX-SR abrasive, after which acetone cleaning was repeated.

All SLJs were tested to failure at a test speed of 1.3 mm/min using an Instron 8802 servo-hydraulic testing machine (Instron, MA, USA).

Laser surface pretreatments

Laser texturing was performed using a nanosecond pulsed Ytterbium-doped fiber laser (Laserpoint Blitz 20P) equipped with a collimator, galvanometric scanning head and f-theta lens. Surface areas of 25 mm × 15 mm were treated, by varying the average laser power (P) and scanning velocity (V). The laser beam followed parallel lines, spaced by a distance H from each other, to cover the entire surface; two scanning directions (α), 0° and 90°, were considered, as shown in Fig. 2a and b, respectively.

The main characteristics of the laser equipment used are listed in

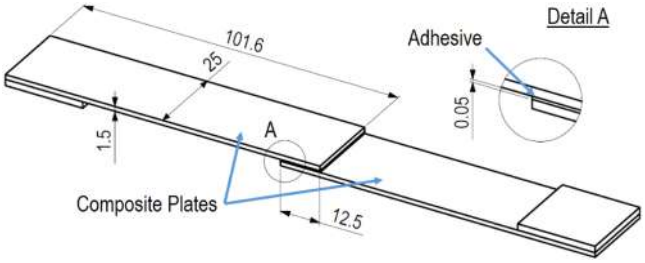

Fig. 1. Single lap joint sample geometry (dimensions in mm).

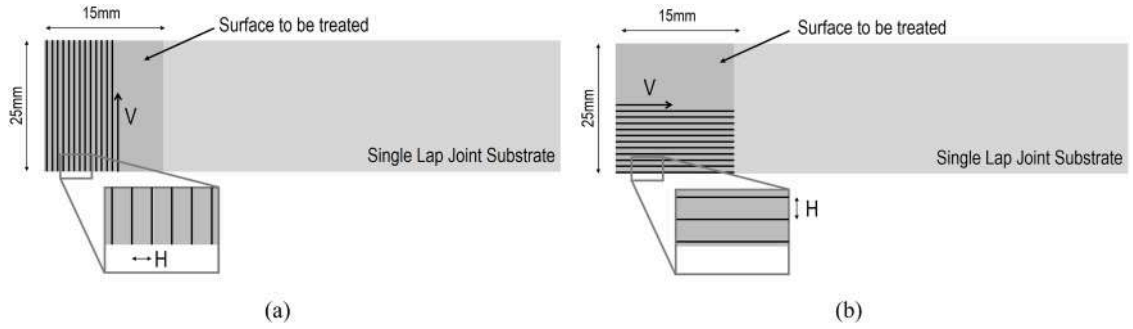

Fig. 2. Scheme of laser scanning path with directions (a) α=0° and (b) α=90°

Table 1
Main characteristics and operating range of laser setup.

Characteristic	Symbol	Type/Value	Unit
Operating mode		Pulse	
Emission wavelength	λ	1064	nm
Pulse duration	τ	104	ns
Repetition frequency	R	20–80	kHz
Nominal Average Power	P	1–17	W
Pulse energy	E_p	12.5–850	μJ
Beam quality (M^2)		1.8	
Focal distance	f	160	mm
Line spacing	H	1–1000	μm
Focused Gaussian spot diameter	d_0	60	μm
Rayleigh length	z_r	1.45	mm
Pulse peak flow	F	0.63–45.8	J/cm^2
Scanning speed	V	0–2500	mm/s
Working area		100 × 100	mm^2

Table 1. The laser beam spot was circular with a focal point beam size (d) of 60 μm and pulse duration (τ) of 104 ns; the pulse repetition frequency (R) was kept constant at 40 kHz.

Precisely, the effects of the laser treatment on the substrate depend on the interactions between different characteristics of the beam so they can be better analyzed by introducing the following parameters:

- the pulse energy (E_p), i.e., the amount of energy delivered for each pulse:

$$E_p = \frac{P}{R} \tag{1}$$

- the fluence (F), i.e., the average amount of energy per unit area delivered for each pulse:

$$F = \frac{4P}{R\pi d^2} = \frac{4E_p}{\pi d^2} \tag{2}$$

- the energy density (E_d), i.e., the average amount of energy delivered for each point lying on the lines where the treatment is performed:

$$E_d = \frac{P}{Vd} \tag{3}$$

The experimental tests were performed following a two-step Analysis of Variance (ANOVA). In the first phase, a model was built following a two-level factorial design, commonly referred to as a 2^2 factorial design augmented with a central point, involving two factors: power (factor A) and speed (factor B), keeping both the distance H and the direction α fixed. These analyses aimed to discern the individual and combined impacts of the process factors on the response variable, namely, the TSS of adhesive-bonded joints. The choice of a two-level factorial design was motivated by the objective of identifying general trends in substrate behavior across varying levels of the process factors.

Once the significance of the main parameters of power and speed was identified, these were combined into a single parameter, E_d, (factor C), which was used as factor alongside the line spacing H and the scanning direction α (factors D and E, respectively) for the second ANOVA analysis. The latter included both TSS and the mean height of ablated material (Z_m) as response variables, aiming to further investigate the thermal effect of the laser on the surface. In this case, a 2^3 factorial design was used, and additional experiments were performed to deepen the investigation regarding the line spacing.

The aforementioned two ANOVA designs can be graphically represented as one square with four treatment combinations situated at its corners and one central point in addition (Fig. 3a) and a cube with four extra points (Fig. 3b), respectively. Three replicates (N=3) were made for each treatment combination to estimate experimental error accurately, assisting in distinguishing statistical differences from random experimental noise.

The two-level factorial design facilitates the creation of a response surface model through linear regression analysis, fitting an appropriate equation to the data. This linear regression model reflects the underlying relationship between the factors investigated and the response variable. Table 2 lists all sets of treatment conditions considered. The process parameter values then correspond to three pulse energy levels, which are tested, along with three line-spacing values. A repetition frequency (R) of 40 kHz was used for all treatments performed.

Surface profilometry and high-resolution imaging

To support the mechanical observations, the effect of the laser texturing on the composite surface morphology was also investigated through surface analyses performed using a CCI MP-L (Taylor Hobson, Leicester, UK) digital optical profilometer. For each treatment considered, a surface area of 4.4 mm × 4.4 mm was scanned, generating morphology maps like the one shown as an example in Fig. 4. All acquisitions were carried out with a resolution of 3.4 μm on the longitudinal plane (XY) and 5 nm along the vertical axis (Z).

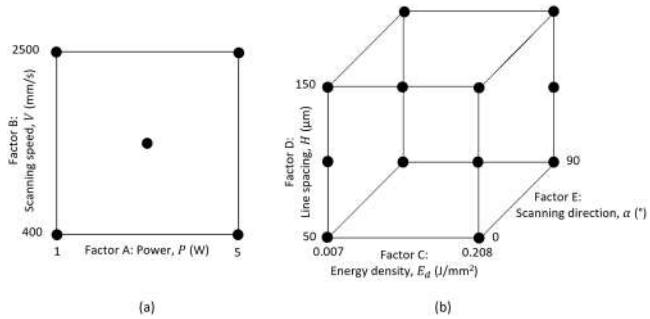

Fig. 3. 2^k factorial designs for (a) k=2, augmented with extra tests, and (b) k=3.

Table 2
Laser processing parameters of experiments and sample designation (R=40 kHz for every sample).

Sample designation	P (W)	V	E_p	F	E_d	H	α
P1_V400_ H50_0°	1	400	0.025	0.88	0.042	50	0
P5_V400_ H50_0°	5	400	0.125	4.42	0.208	50	0
P3_V1000_ H50_0°	3	1000	0.075	2.65	0.050	50	0
P1_V2500_ H50_0°	1	2500	0.025	0.88	0.007	50	0
P5_V2500_ H50_0°	5	2500	0.125	4.42	0.033	50	0
P5_V400_ H100_0°	5	400	0.125	4.42	0.208	100	0
P5_V400_ H150_0°	5	400	0.125	4.42	0.208	150	0
P1_V2500_H100_0°	1	2500	0.025	0.88	0.007	100	0
P1_V2500_H150_0°	1	2500	0.025	0.88	0.007	150	0
P5_V400_ H50_90°	5	400	0.125	4.42	0.208	50	90
P5_V400_ H100_90°	5	400	0.125	4.42	0.208	100	90
P5_V400_ H150_90°	5	400	0.125	4.42	0.208	150	90
P1_V2500_ H50_90°	1	2500	0.025	0.88	0.007	50	90
P1_V2500_H100_90°	1	2500	0.025	0.88	0.007	100	90
P1_V2500_H150_90°	1	2500	0.025	0.88	0.007	150	90

For some specific treatments, detailed SEM images were also taken by using a Field-Emission SUPRA40 Zeiss SEM equipped with a GEMINI FESEM detection column.

Evaluation of ablation rate

To correlate the mechanical performance of the joints to the treatment settings, the amount of material ablated during the process was estimated. For this purpose, all profilometric scans were performed in such a way as to include a portion of the untreated surface within the morphological map acquired, as shown in Fig. 5. The original untreated surface was taken as a reference to define the amount of material ablated.

As observable in Fig. 5a, the treatment caused heterogeneous ablation of the composite material. In most of the treated area, the ablation affected the matrix, exposing the fibers and resulting in a lowering of the surface (A) compared with the reference untreated one. In contrast, in portions corresponding to the fiber interweave locations (B), the treatment did not significantly change the surface. Finally, in small portions (C) at the edge between the areas A and B, localized heating caused the exposed fibers to rise even above the level of the reference surface. As will be better explained in later sections, this uneven behavior is likely related to the epoxy matrix, precisely, its nonuniform distribution (thickness) over the measured area and its transparency at the laser wavelength, which makes ablation indirect.

Based on this, the area A alone was considered to compute the average amount of ablated material (Fig. 5b); since the data generating the morphology maps were available in terms of *xyz* coordinates of the surface, the mean height of ablated material was computed as per **Eq. (4)**:

$$Z_m = \frac{\sum_{x=i}\sum_{y=j}\overline{z_{ij}}}{n} \tag{4}$$

where

$$\overline{z_{ij}} = \begin{cases} z_{ij} & \text{if } z_{ij} \leq -0.5\ \mu\text{m} \\ \text{not considered} & \text{elsewhere} \end{cases}$$

and n is the number of points where $\overline{z_{ij}}$ was considered. The value of 0.5 μm was assumed as a threshold to exclude the surface unevenness from the calculation.

In addition to the calculation of the mean height of ablated material, the roughness parameters were extracted from the areal acquisitions (by excluding the reference untreated surface) in accordance with the EN ISO 25178 (British Standards Institution n.d.) standard, among which the arithmetical mean height S_a of the laser treated portion of each acquired surface was selected to be provided as a result.

Results and discussion

Morphology and ablation rate evaluation

This section deals with the effect of laser treatment on the morphology of the composite material, as a function of the process parameters. Fig. 6 compares the morphological maps of surfaces treated with laser treatments performed by varying the average power (P) and the scanning speed (V), for a constant line spacing value (H=50 μm). Both variable parameters played a significant role in surface modification, although the average power appeared to have a more pronounced effect. The surfaces treated with the higher laser power showed significant ablation of the matrix and damage of the outer layer of the fibers. Moreover, in some locations, the fibers were raised over the original plane. For the lower power value, the amount of ablation was much less: the fiber raising almost completely disappeared at the highest velocity, while only a small amount of ablation of the matrix resin occurred at the lowest velocity.

A further comparison is made in Fig.7 where the effect of the line spacing is shown, for the same average power (P=5 W) and scanning speed (V=400 mm/s). The surface treated with the lowest line spacing

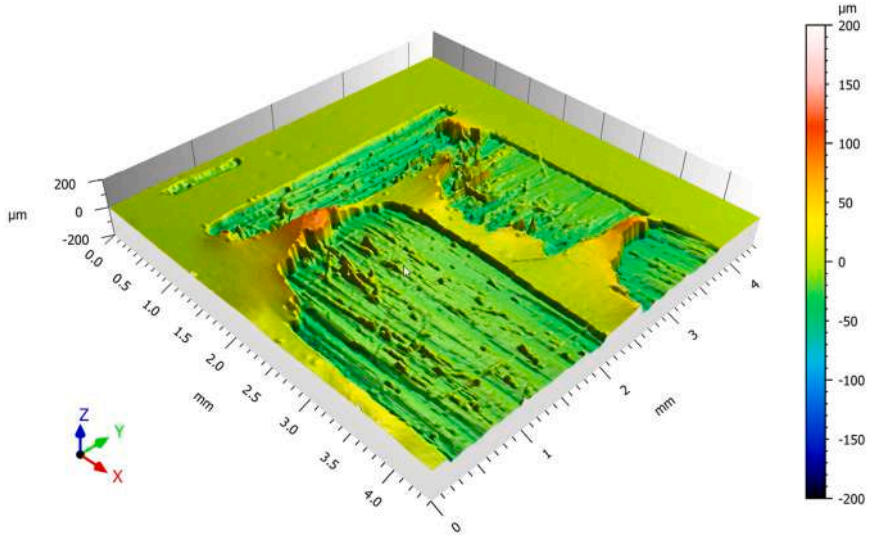

Fig. 4. Example of morphology map of a laser treated CFRP surface portion acquired using digital optical profilometer.

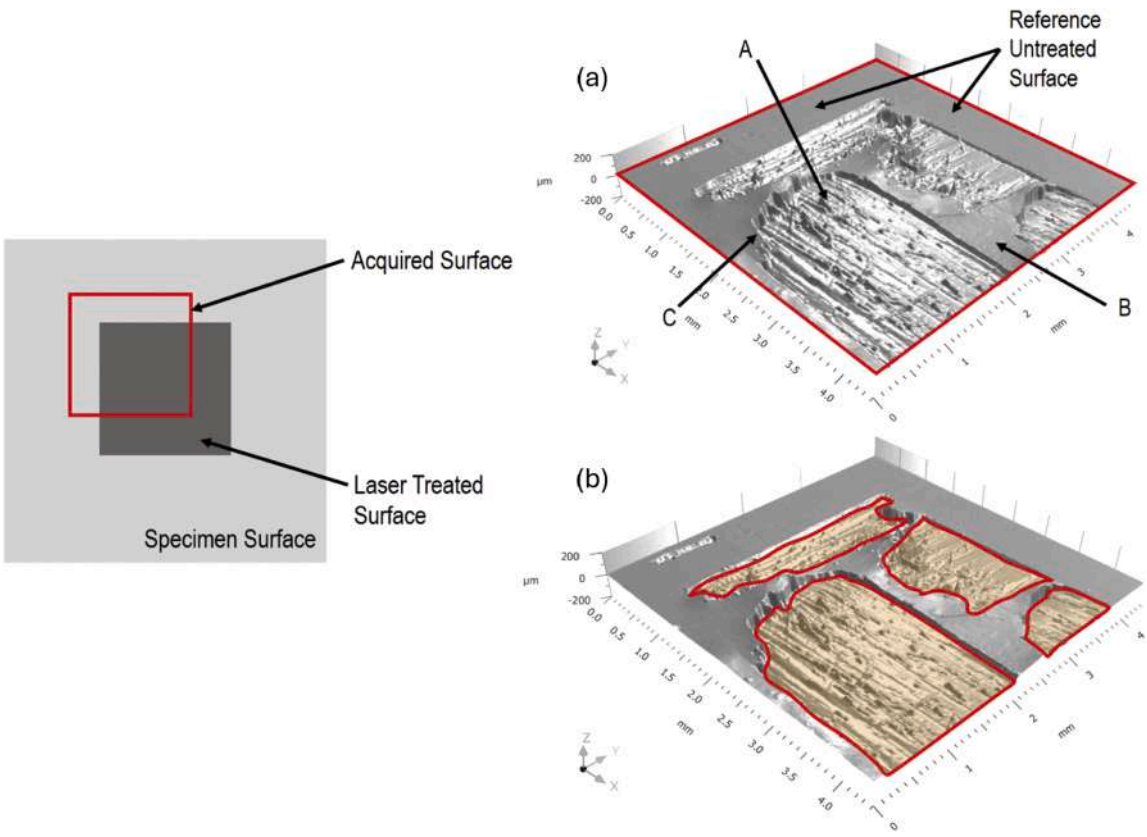

Fig. 5. Detail of areal scan position for evaluation of the ablated surface with respect to the reference untreated surface.

resulted quite homogeneous (without any visible footprint of the scanning direction): the value of the line spacing (H=50 μm) was lower than the laser spot diameter (d=60 μm) and therefore the surface was completely irradiated by the laser beam. On the contrary, for the wider line spacing, the surface was characterized by clearly separated grooves produced by the laser beam.

In order to better understand the result of the treatment, SEM images are provided in Fig. 8. Specifically, Fig. 8a shows the appearance of surfaces treated with the highest power (P=5 W), the lowest velocity (V=400 mm/s) and narrowest line spacing (H=50 μm), which corresponds to the condition characterized by the highest values of Pulse Energy, Fluence and Energy Density. It is quite clear that the outer matrix layer was completely removed and the fibers fully exposed.

Furthermore, it can be noted that several fibers were broken and damaged, and there was a great deal of debris on the surface. Decreasing the average power to 1 W (Fig. 8b) led to a significant reduction in the amount of the ablation, even though small portions of the matrix were still removed. Fibers were exposed in some places; however, they did not appear to be significantly damaged.

The increase of the scanning speed up to 2500 mm/s (Fig. 8c) made the distance between subsequent pulses larger than the laser spot diameter. Therefore, the pulses were separated from each other and could be identified over the surface (pulses pointed out by the black arrows). The ablation was restricted to an area corresponding to the single pulses, and no significant fibers damage can be identified.

Finally, when the line spacing was increased to H=100 μm, namely, above the size of the laser spot (Fig. 8d), the grooves produced on the surface presented the same features already shown for sample P1_V400_H50: the matrix was ablated and the fibers exposed, resulting in significant damage. However, the portion of the matrix between the grooves showed no apparent considerable modifications, although much debris of damaged fibers could be found on it.

The analysis of the surface morphology and the SEM observations allowed a better understanding of the ablation process: as also confirmed by some literature works (Feng et al., 2021; Harder et al., 2019), due to the partial transparency of the matrix for the specific laser wavelength, most of the energy was absorbed by the fibers, and then transferred to the resin, causing the vaporization of the latter. Near the bundle interweaves, the thickness of the matrix increases locally, reducing the amount of energy transferred to the fibers, and therefore reducing the ablation phenomenon.

Fig. 9 shows the average thickness of ablated material (Z_m) and the value of the average surface roughness (S_a) as a function of the energy density (E_d). To determine a trend for these parameters, four additional laser parameter combinations were considered in addition to those reported in former Table 2, precisely: P3_V400_H50_0° (E_d=0.125 J/mm^2), P1_V1000_H50_0° (E_d=0.017 J/mm^2), P5_V1000_H50_0° (E_d=0.083 J/mm^2), and P3_V2500_H50_0° (E_d=0.020 J/mm^2). It is quite clear that, when the entire surface is covered by the treatment (H=50 μm), Z_m increases with increasing E_d (Fig. 9a). An increasing trend was also found by plotting the S_a parameter as a function of E_d (Fig. 9b), although it was more scattered than the former. In contrast, pulse energy (E_p) and fluence (F) did not show a direct relationship with the surface parameters, as they are formally independent of the scan speed parameter, which was instead shown to be relevant to the ablation process.

Effect of laser surface treatment on lap shear strength

The two sets of RJs were preliminary tested to provide a reference against which to evaluate the performance of the laser-treated joint series. As shown in Table 3, mechanical abrasion treatment determined an increase of 13.4 % in TSS of joints compared to the degreased-only counterpart.

The experimental TSS values obtained from testing the laser-treated SLJs series with different treatment conditions are reported in Table 4,

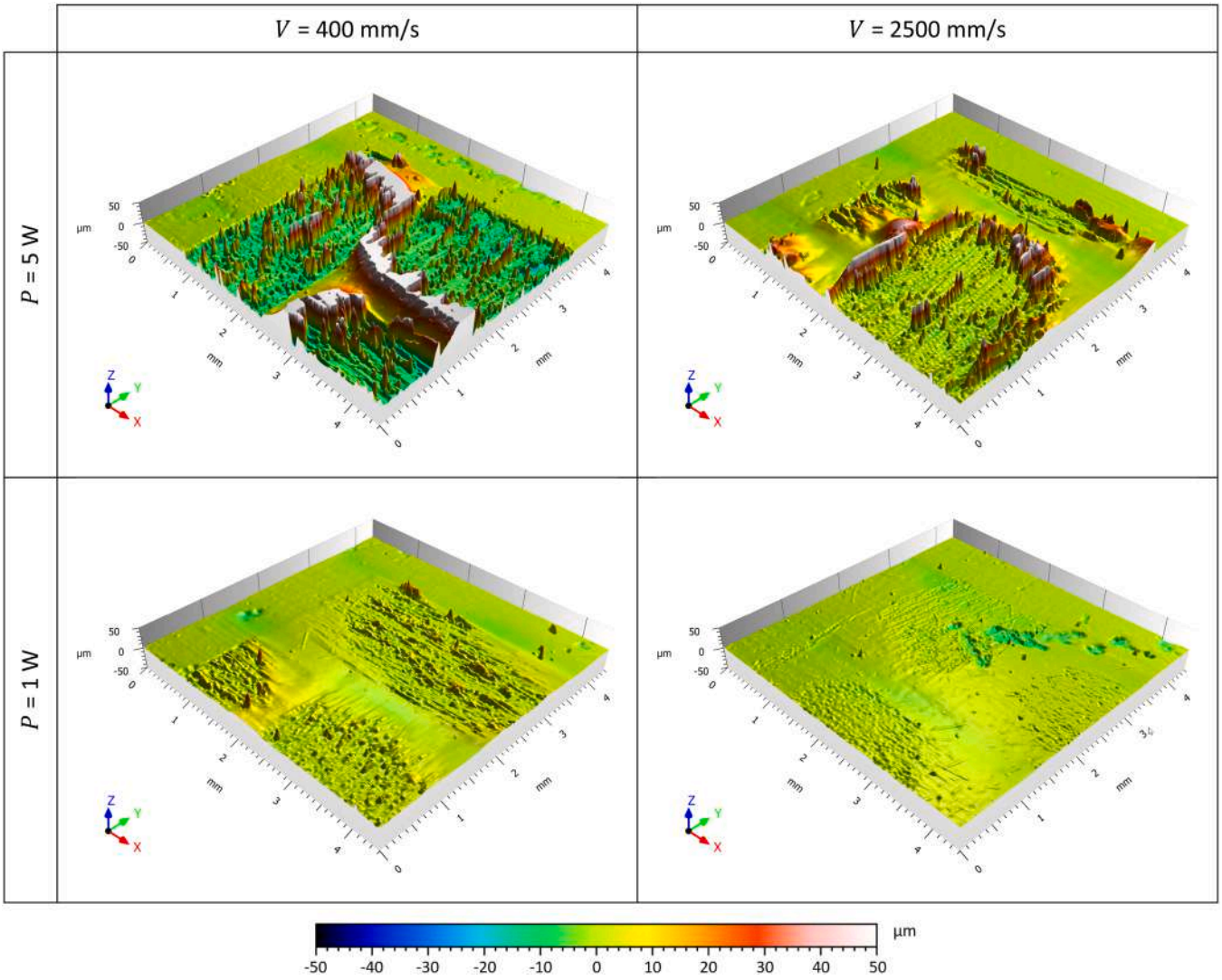

Fig. 6. Morphology maps acquired after the laser treatment for different values of power (P) and scanning speed (V), for the same line spacing (H=50 µm).

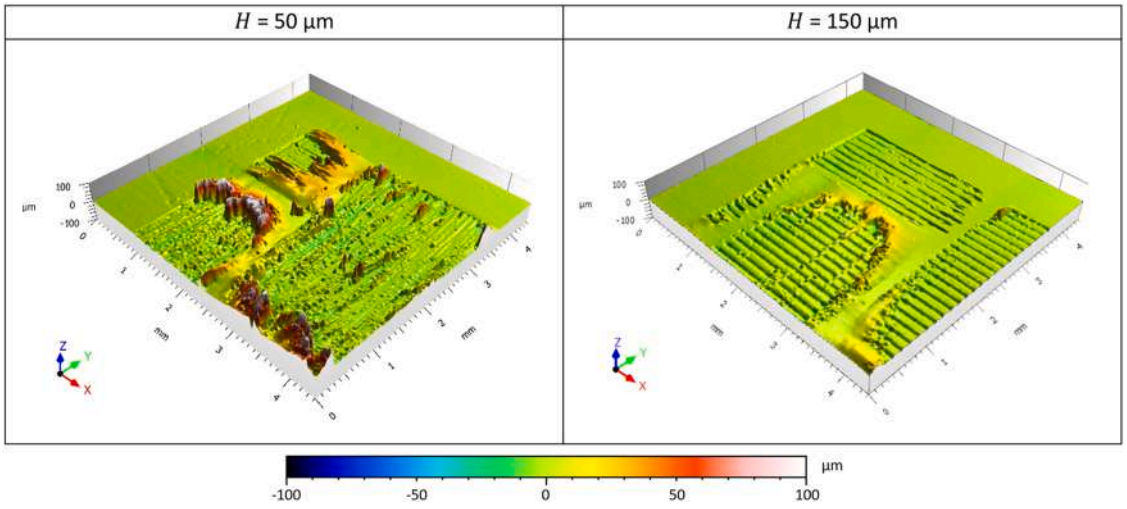

Fig. 7. Morphology maps acquired after the laser treatment for different values of line spacing H, for the same power (P=5 W) and scanning speed (V=400 mm/s).

in which the relative differences are those of the mean values of ultimate TSS against the two references. Specifically, improvements in TSS of the laser-treated SLJs were found in 10 and in 7 out of 15 cases when compared to the degreased and the abraded RJs, respectively.

A preliminary statistical analysis over the mechanical results was performed to evaluate the effect of the main laser parameters (namely,

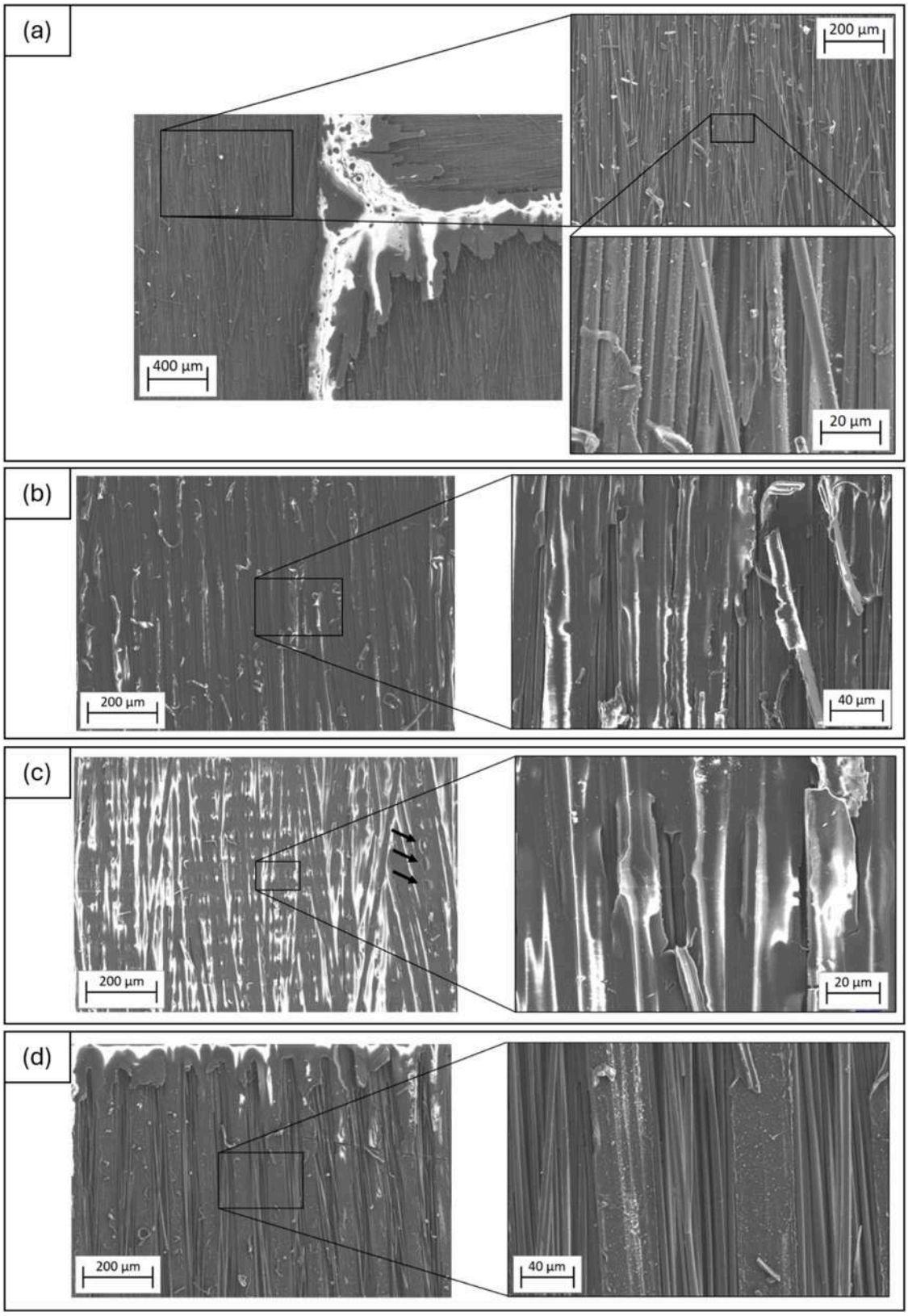

Fig. 8. SEM images of the surface of samples (a) P5_V400_ H50, (b) P1_V400_ H50, (c) P1_V2500_ H50, and (d) P1_V400_ H100.

power and speed) on joint strength. The ANOVA (Table 5) resulted in a significant model (F-value of 17.34). A 2^2-factorial design enters each factor's first-order effect (indicated as A and B respectively) along with the first-order interaction between the factors (AB). Aiming at a significance level of 0.1, *p*-values greater than 0.1000 indicate the model terms are not significant. In this case A and B are significant model term values. Notably, Power exhibited the most prominent impact on the increase in TSS values, while the interaction effect, which was not

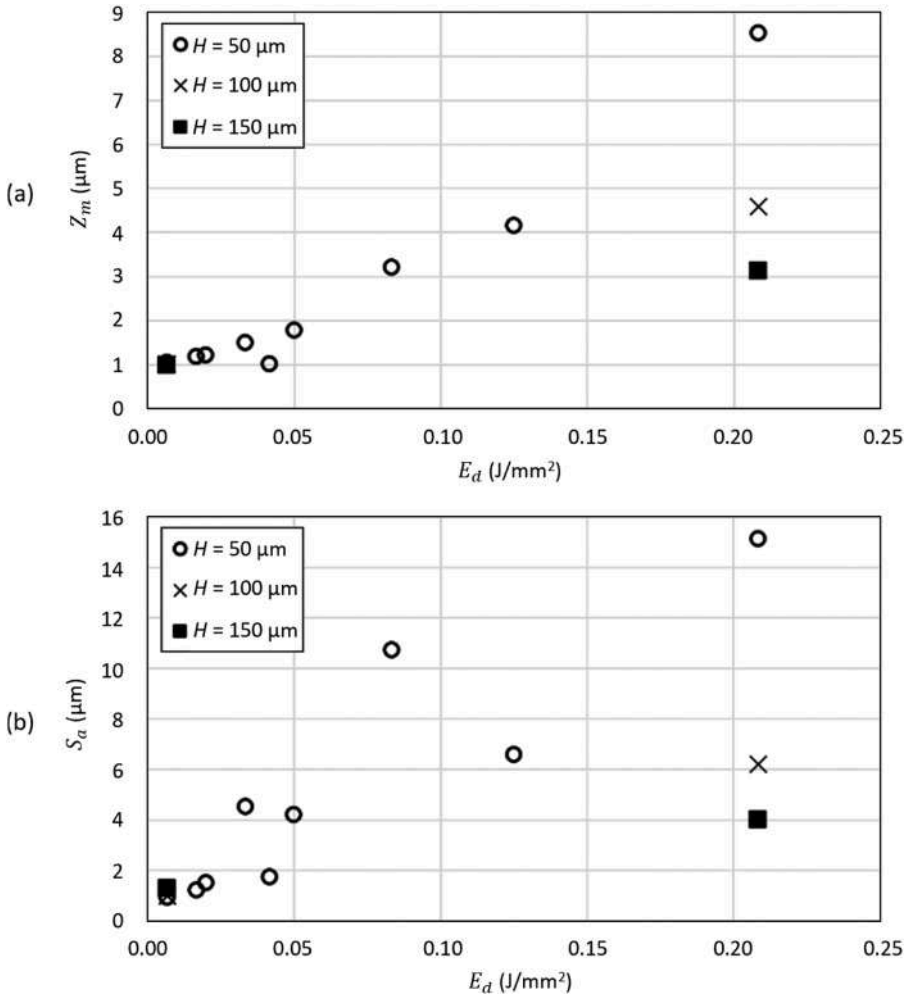

Fig. 9. (a) Average thickness of ablated material, Z_m, and (b) average surface roughness, S_a, as a function of the energy density, E_d.

Table 3
Tensile shear strength of the RJs.

Treatment	TSS (MPa)	STD (%)
Degreasing	22.66	33.94
Abrasion	25.69	4.67

Table 4
Tensile shear strength of the laser-treated SLJs.

Sample designation	Average TSS (MPa)	Std Dev (%)	TSS vs. degreased RJ (%)	TSS vs. abraded RJ (%)
P1_V400_ H50_0°	25.12	12.07	10.9	-2.2
P5_V400_ H50_0°	17.76	1.83	-21.6	-30.9
P3_V1000_ H50_0°	19.82	5.48	-12.5	-22.8
P1_V2500_ H50_0°	26.89	5.00	18.7	4.7
P5_V2500_ H50_0°	20.67	4.43	-8.8	-19.5
P5_V400_ H100_0°	24.12	0.47	6.4	-6.1
P5_V400_ H150_0°	19.08	4.19	-15.8	-25.7
P1_V2500_H100_0°	29.98	4.45	32.3	16.7
P1_V2500_H150_0°	29.64	2.63	30.8	15.4
P5_V400_ H50_90°	21.09	6.81	-6.9	-17.9
P5_V400_ H100_90°	27.69	5.27	22.2	7.8
P5_V400_ H150_90°	26.07	4.05	15.0	1.5
P1_V2500_ H50_90°	24.37	9.64	7.5	-5.1
P1_V2500_H100_90°	26.58	2.82	17.3	3.5
P1_V2500_H150_90°	27.39	4.28	20.9	6.6

significant, was merged into the Residual Variance.

Additionally, the Lack of Fit was not significant, indicating that the first-order linear regression model expressed by **Eq. (5)** adequately fit the experimental values. This equation correlates the expected TSS of the joints realized with laser-treated substrates to the P and V laser parameters, reported in coded variables with +1 for a high level and –1 for a low level.

$$TSS = 22.21 - 3.45P + 1.31V \quad (5)$$

It should be mentioned that coding offers two benefits: first, it standardizes the factors to a uniform magnitude, simplifying the assessment of each factor's relative significance; second, it positions the model intercept, β_0, at the experimental design's center. Regression coefficients in **Eq. (5)** suggest a positive effect of the speed, while increase of power had a negative effect on TSS.

In Fig. 10a, the first-order response surface is displayed in a three-dimensional wireframe, while Fig. 10b shows the interaction plot.

From the ANOVA and response surface, it can be concluded that, to obtain high-quality adhesive bonded joints, it is necessary to limit laser power and use high scanning speeds. This leads to the assumption that excessive heat input and, consequently, high energy transferred to the substrate surface affect the joint performance negatively. This observation well complements what resulted from the morphology analysis, where it was found that exposure to treatments characterized by high energy density results in complete removal of the polymer matrix and partial damage to the reinforcing fibers, as detailed in former Fig. 6.

With these premises, a second ANOVA was conducted, considering

Table 5
Results of the ANOVA performed by considering *P* and *V* parameters.

Source	Sum of squares	Degrees of freedom	Mean square	F-value	*p*-value	
Model	164.20	2	82.10	19.67	0.0002	significant
A- Power, *P*	142.90	1	142.90	34.23	<0.0001	
B- Scanning speed, *V*	21.30	1	21.30	5.10	0.0433	
Residual	50.10	12	4.17			
Lack of Fit	14.40	2	7.20	2.02	0.1837	not significant
Pure Error	35.70	10	3.57			
Cor Total	214.29	14				

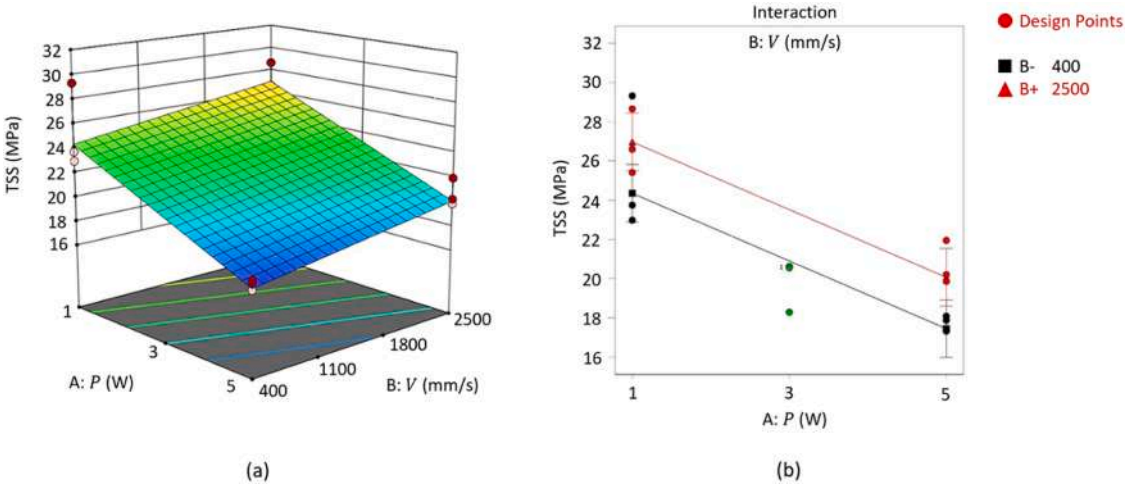

Fig. 10. (a) Response surface of laser-treated and (b) interaction plot.

the energy density parameter, E_d, and evaluating the effect of those geometrical parameters that are assumed to play a key role in the substrate heating, despite not being included in the formula for E_d. Specifically, *P* and *V* parameters were merged into the single parameter E_d, and the analysis focused also on parameters such as line spacing, *H*, and scanning direction, α, to obtain information about the possibility of intervening in their adjustment to limit substrate heating and improve joint performance. In this regard, both the TSS and Z_m responses were considered.

As for the TSS response (Table 6), some tests had to be excluded to fit the model, particularly those with spacing H=100 μm. Confirming the findings from the previous model, E_d is the most significant factor, followed by line spacing *H*. In turn, the scanning direction α does not influence the variation of mechanical performance, resulting in a non-determining factor for the reduction of thermal input on the material.

From the coded-factor Eq. (6) describing the trend of TSS, further confirmation of what was deduced from the previous model is found; indeed, to maximize mechanical resistance, it is necessary to combine low energy values with a high spacing between passes.

$$TSS = 24.04 - 3.04E_d + 1.51H + 0.69\alpha + 0.06E_dH + 1.89E_d\alpha + 0.49H\alpha \quad (6)$$

The response surfaces (Fig. 11) highlight that improvements in mechanical properties were achieved, even higher than the setups used to create the previous model. This can be considered a positive aspect even from the perspective of process sustainability. Indeed, maintaining low energy density values results in a lower-consumption treatment, and spacing the treatment lines drastically reduces the total process duration, with undoubted advantages in terms of process productivity, especially in the case of applications requiring the treatment of large surfaces.

To assess the effect that E_d, *H*, and α parameters have on the amount of ablated material (i.e., Z_m parameter), the same factorial design was used, and the ANOVA result is reported in Table 7.

In this case, both E_d and *H* are significant model term values, as well as the combined effect of the two factors, while scanning direction α has

Table 6
Results of the ANOVA performed by considering E_d, *H*, and α parameters: TSS response.

Source	Sum of squares	Degrees of freedom	Mean square	F-value	*p*-value	
Model	378.55	6	63.09	24.39	<0.0001	significant
C-E_d	221.13	1	221.13	85.49	<0.0001	
D-Spacing, *H*	54.51	1	54.51	21.07	0.0003	
E-Direction, α	11.55	1	11.55	4.47	0.0497	
CD	0.10	1	0.10	0.04	0.8444	
CE	85.47	1	85.47	33.04	<0.0001	
DE	5.79	1	5.79	2.24	0.1529	
Residual	43.97	17	2.59			
Lack of Fit	4.33	1	4.33	1.75	0.2050	not significant
Pure Error	39.65	16	2.48			
Cor Total	422.53	23				

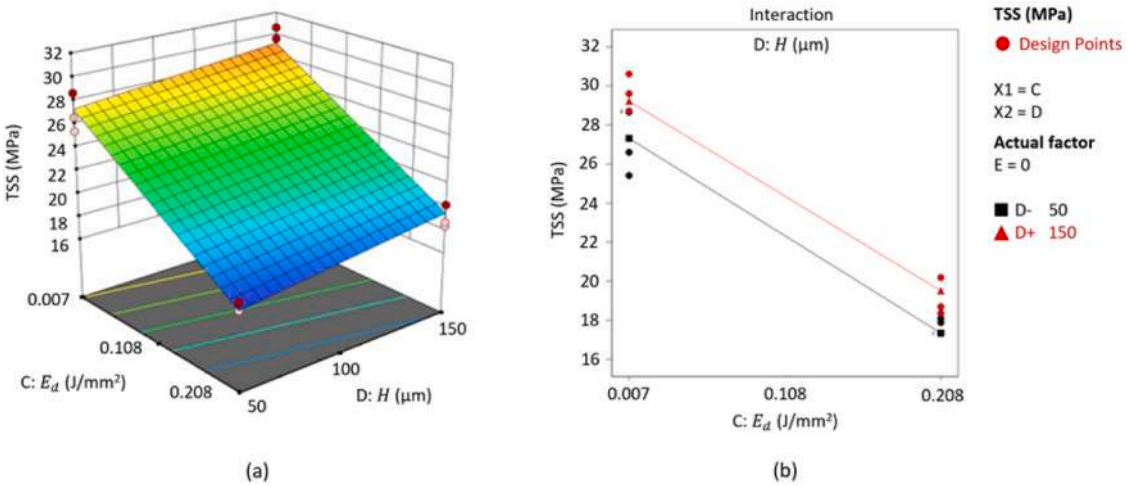

Fig. 11. (a) Response surface of laser-treated samples with a 0° scanning direction and (b) interaction plot.

no influence on the ablated material. Moreover, the Lack of Fit was not significant, so the first-order model fitted the experimental values. The values of Z_m within the domain can be deduced from **Eq. (7)**, again expressed in coded factors.

$$Z_m = 3.22 + 2.20E_d - 1.36H - 1.33E_dH \quad (7)$$

As shown in Fig. 12, the trend is contrary to that obtained in the previous case where TSS was evaluated as the response, as can also be deduced by comparing the (opposite) signs of factors between **Eq. (7)** and former Eq. (6).

The results obtained emphasized that the mechanical behavior of adhesive joints appears to be strictly related to the amount of ablated material. In this regard, a correlation between the two response variables was determined via Design Expert analysis software in order to quantitatively estimate how the degree of ablation influences the mechanical strength of the adhesive bonded joints. From the scatter plot displayed in Fig. 13, a negative correlation coefficient of -0.663 was estimated. Comparing the results obtained with laser-treated SLJs with those obtained with the abraded RJs (horizontal reference line corresponding to 25.69 MPa), it is deduced that the performance improvement of joints due to laser treatment is contingent on maintaining the Z_m parameter value below a certain threshold, in this case determined equal to 3.5 μm, i.e., approximately the thickness of the matrix on the upper surface of the CFRP substrate. In other terms, the effect of laser treatment on the final joint strength is positive as long as treatment involves ablation of the polymer matrix without exposing the underlying fibers.

Fracture surface and SEM analysis

To better understand the failure mechanisms of bonded joints and the influence of the laser treatment on the result in terms of TSS, the fracture surfaces of specimens were investigated by both optical and SEM observations. Fig. 14 shows the three different failure behaviors presented by the laser-treated samples.

Sample P5_V400_H50_0° exhibited predominant substrate failure; as can be seen in the corresponding SEM image in Fig. 15a, the fractured surface presented a layer of broken fibers (red arrows) at the outmost layer. In addition, the fibers showed extensive damage in the interleaving zone (white arrows), where a significant portion of the damaged material (resin and fibers) was torn away. In other words, the laser treatment significantly damaged the fiber bundles, and the fracture of the joints was mainly related to their out-of-plane failure.

Fig. 15b, shows an SEM image of the fracture surface of a P1_V400_H50_0° specimen. In this case, failure was mainly adhesive in type (at the areas affected by exposed fibers), with only a small portion of substrate failure (where the weak layer of matrix damaged by the laser treatment was torn out). Globally, this resulted in significant fiber exposure without substantial damage to the fiber bundles.

Finally, in case of P1_V2500_H100_0° sample (Fig. 15c), mixed adhesive-cohesive and substrate failure occurred. Indeed, it is possible to recognize portions of highly deformed adhesive resin (red arrows), as well as exposed fibers (white arrows). It is worth noting that this case, where at least part of failure occurred within the adhesive layer (cohesive failure), corresponds to the one that showed the highest TSS values among the laser-treated SLJs tested: this observation suggests that the laser treatment was able to create a good bonding conditions at the interface between CFRP and adhesive, without overdoing the exposure or damage of the fibers reinforcing the composite substrate.

Conclusions

This study explored the impact of process parameters associated with nanosecond pulsed laser pre-bonding surface treatment on the ablation process of an epoxy-matrix CFRP. Through a comprehensive experimental activity, the aim was to attain optimal ablation while minimizing fiber damage. Specifically, the relationship between the amount of ab-

Table 7
Results of the ANOVA performed by considering E_d, H, and α parameters: Z_m response.

Source	Sum of squares	Degrees of freedom	Mean square	F-value	p-value	
Model	261.36	3	87.12	151.47	<0.0001	significant
C-E_d	174.08	1	174.08	302.67	<0.0001	
D-Spacing, H	44.62	1	44.62	77.59	<0.0001	
CD	42.65	1	42.65	74.16	<0.0001	
Residual	18.40	32	0.58			
Lack of fit	6.16	8	0.77	1.51	0.2060	not significant
Pure error	12.24	24	0.51			
Cor total	279.76	35				

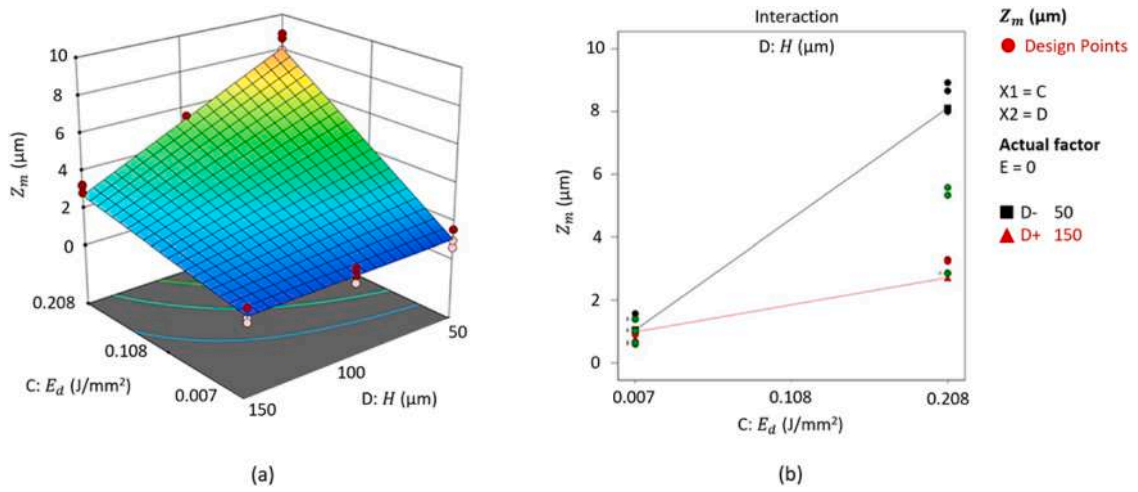

Fig. 12. (a) Response surface of laser-treated samples with a 0° scanning direction and (b) interaction plot.

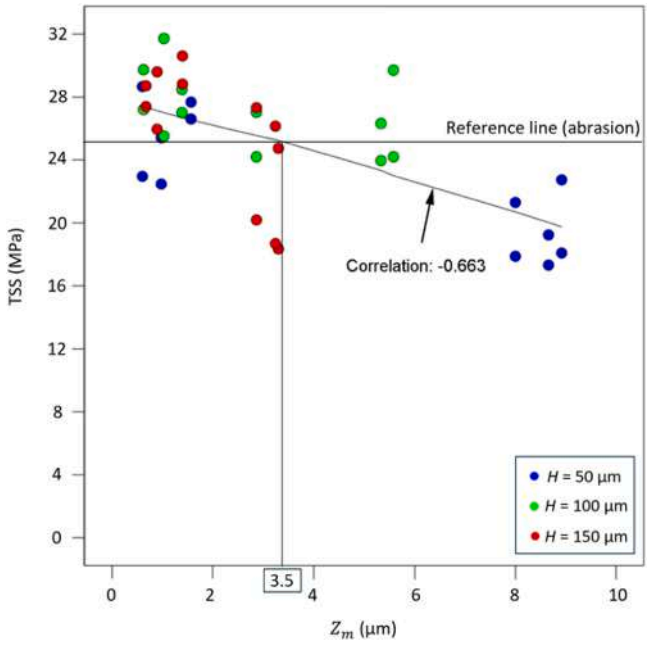

Fig. 13. Scatterplot representing the correlation between TSS and Z_m color by line spacing.

lated material and the tensile shear strength of adhesive-bonded joints was examined using profilometer surveys, tensile shear tests, and SEM analysis. The following key conclusions emerged:

- The experimental findings of surface investigation performed by profilometry showed that average power (P) has a greater influence on surface modification than scanning speed (V). Performing high P laser treatments resulted in significant ablation of both the matrix and damage of the outer layers fibers, with some fibers raised above the original surface plane. Conversely, lower P values resulted in reduced ablation, with minimal matrix removal when combined with higher values of the V parameter. Further investigation of the effect of line spacing (H) revealed distinct surface features, with narrower spacings producing more homogeneous surfaces, while wider spacings generated clearly separated grooves. SEM images provided deeper insights, showcasing complete removal of the outer matrix layer and exposure of fibers under specific treatment conditions.
- Statistical analyses, including ANOVA, highlighted the influence of laser parameters on lap shear strength (TSS) of joints. P parameter emerged as the predominant factor affecting TSS, while V parameter confirmed to have a secondary effect also in this case. The regression models, validated by Lack-of-Fit tests, provided predictive insights into TSS behavior, guiding optimization efforts. Subsequent analysis combined power and speed into energy density (E_d), revealing its pivotal role in joint strength. Additionally, line spacing (H) emerged as a significant factor, while scanning direction (α) showed negligible

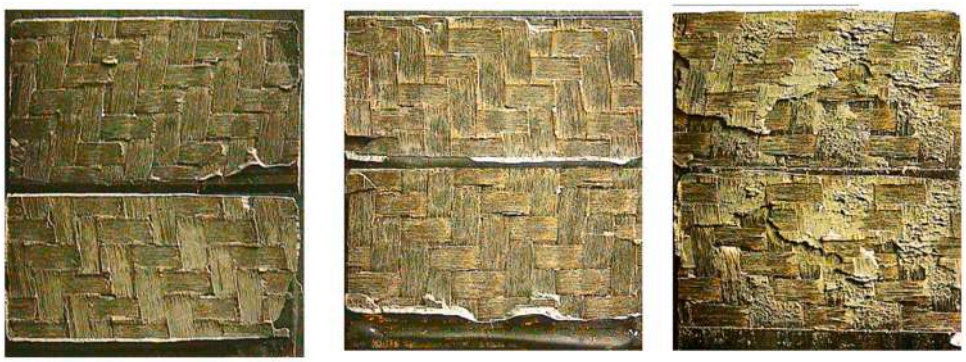

Fig. 14. Fracture surfaces of three representative specimens with three different failure behaviors.

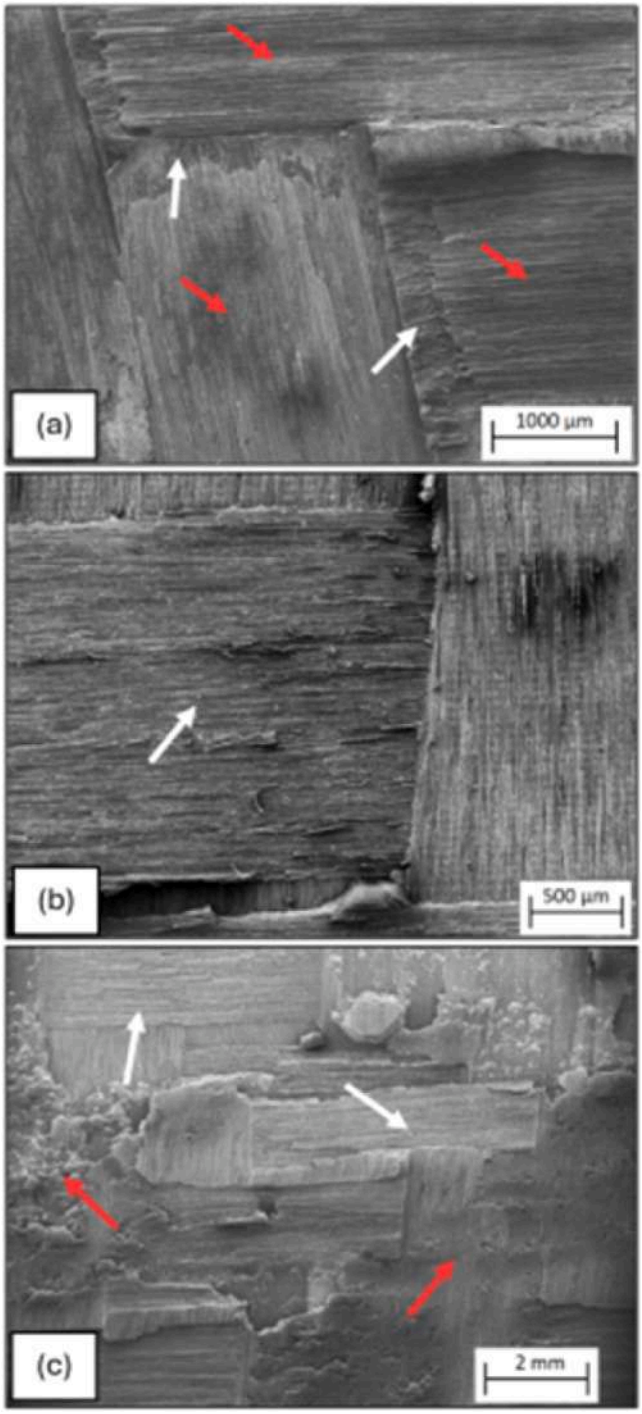

Fig. 15. SEM images of the fracture surfaces of samples (a) P5_V400_H50_0°, (b) P1_V400_H50_0°, and (c) P1_V2500_H100_0°.

influence. Correlation analyses highlighted a negative relationship between TSS and ablated material thickness (Z_m), suggesting the importance of controlling ablation for joint integrity.

- Analyses of the fracture surfaces revealed different failure mechanisms, with laser treatment inducing failure of the substrate, adhesive, or mixed modes depending on specific parameters adopted. SEM observations emphasized the delicate balance between fiber exposure and matrix integrity, which is crucial for optimal joint performance.

Summarizing these observations, the P1_V2500_H100_0° series resulted in the best performing laser parameter combination among those investigated, allowing for joints characterized by a TSS value of +16.7 % compared to reference abraded joints. Interestingly, although statistically significant, this improvement is not excessively large. From an application point of view, this suggests that pulsed laser treatment of CFRP is still advantageous in those contexts where higher productivity, degree of automation and process repeatability are required, justifying the higher process costs compared to mechanical abrasion. From a process perspective, the experimental and statistical findings highlighted that there exists a pathway to enhance the mechanical strength of laser-treated joints. Achieving this goal is dependent on a multitude of factors that collectively contribute to the overall quality of the joint. A key factor is Z_m, which serves as an initial indicator and provides a quantitative measure of the treatment's potential efficacy. Optimal results are achieved when Z_m remains within a specific range, facilitating successful ablation without damaging the fibers. This delicate balance ensures that the joint retains its integrity and strength. Conversely, when Z_m exceeds its optimal threshold, it can lead to the unintended consequence of fiber damage, resulting in a decline in the joint's tensile strength.

The relationship that links Z_m to the energy density and the spacing between passes proves to be a valuable tool that can offer insights into the various process factors at play. By providing a means to estimate these factors, it allows for more precise management of process parameters.s

Furthermore, the correlation established between ablated material and energy dose proves invaluable for practitioners grappling with process optimization. By avoiding the reliance on absolute values of power and speed, this approach offers a more general understanding of how to manipulate parameters effectively, regardless of the laser equipment and/or features of the source employed.

Statements and declarations

The authors declare that no funds, grants, or other support were received during the preparation of this manuscript. The authors have no relevant financial or non-financial interests to disclose.

CRediT authorship contribution statement

Chiara Mandolfino: Writing – review & editing, Writing – original draft, Methodology, Investigation, Data curation, Conceptualization. **Fabrizio Moroni:** Writing – review & editing, Methodology, Investigation, Data curation, Conceptualization. **Marco Pizzorni:** Writing – review & editing, Writing – original draft, Investigation, Conceptualization.

Declaration of competing interest

The authors declare that they have no known competing financial interests or personal relationships that could have appeared to influence the work reported in this paper.

References

ASTM International, D5868-01(2023): standard test method for lap shear adhesion for fiber reinforced plastic (FRP) Bonding, (n.d.).

Bora, M.Ö., Akman, E., Çoban, O., Genc Oztoprak, B., Demir, A., 2019. The effect of CO2 laser-induced microhole formations on adhesive bonding strength of CFRP/CFRP joints. Polym. Compos. 40, 2891–2900. https://doi.org/10.1002/pc.25119.

British Standards Institution, Geometrical product specifications (GPS). Surface texture: areal. Part 2, Terms, definitions and surface texture parameters., (n.d.) 74.

Bénard, Q., Fois, M., Grisel, M., 2007. Roughness and fibre reinforcement effect onto wettability of composite surfaces. Appl. Surf. Sci. 253, 4753–4758. https://doi.org/10.1016/j.apsusc.2006.10.049.

del Real, J.C., Ballesteros, Y., Chamochin, R., Abenojar, J., Molisani, L., 2011. Influence of surface preparation on the fracture behavior of acrylic adhesive/CFRP composite joints. J. Adhes. 87, 366–381. https://doi.org/10.1080/00218464.2011.562114.

3MTM, Scotch-WeldTM EPXTM Adhesive DP490 Data Sheet, n.d.

Favi, C., Moroni, F., Lutey, A.H.A., Rodríguez, N.B., 2021. LCA of laser surface activation and traditional pre-treatments for adhesive bonding of engineering polymers. Procedia CIRP. Elsevier B.V., pp. 541–546. https://doi.org/10.1016/j.procir.2021.01.148

Feng, Z., Zhao, H., Tan, C., Zhang, X., Chen, B., Song, X., 2021. Nanosecond laser ablation for improving the strength of CFRTP and aluminum alloy adhesively bonded joints. Compos. Struct. 274. https://doi.org/10.1016/j.compstruct.2021.114369.

Gomes, F., Baptista, A.P.M., Pinto, A.M.G., Magalha, A.G., 2008. Shear strength of adhesively bonded polyolefins with minimal surface preparation. Int. J. Adhes. Adhes. 28, 452–456. https://doi.org/10.1016/j.ijadhadh.2008.04.003.

Harder, S., Schmutzler, H., Hergoss, P., Freese, J., Holtmannspötter, J., Fiedler, B., 2019. Effect of infrared laser surface treatment on the morphology and adhesive properties of scarfed CFRP surfaces. Compos. Part A Appl. Sci. Manuf. 121, 299–307. https://doi.org/10.1016/j.compositesa.2019.02.025.

Kanerva, M., Saarela, O., 2013. The peel ply surface treatment for adhesive bonding of composites: a review. Int. J. Adhes. Adhes. 43, 60–69. https://doi.org/10.1016/j.ijadhadh.2013.01.014.

Mandolfino, C., Lertora, E., Pizzorni, M., Gambaro, C., 2021. Laser-induced modification of surface properties by micro- and nano-scale processing. Laser Micro- and Nano-Scale Processing. IOP Publishing, p. 5. https://doi.org/10.1088/978-0-7503-1683-5ch5. –1 to 5–21.

Molitor, P., Barron, V., Young, T., 2001. Surface treatment of titanium for adhesive bonding to polymer composites: a review. Int. J. Adhes. Adhes. 21, 129–136. https://doi.org/10.1016/S0143-7496(00)00044-0.

Moreno, P., Méndez, C., García, A., Arias, I., Roso, L., 2006. Femtosecond laser ablation of carbon reinforced polymers. Appl. Surf. Sci. 252, 4110–4119. https://doi.org/10.1016/j.apsusc.2005.06.008.

Moroni, F., Romoli, L., Khan, M.M.A., 2018. Design of laser-textured surfaces to enhance the strength of adhesively bonded joints. Int. J. Adhes. Adhes. 85, 208–218. https://doi.org/10.1016/j.ijadhadh.2018.06.001.

Prolongo, S.G., Ureña, A., 2009. Effect of surface pre-treatment on the adhesive strength of epoxy-aluminium joints. Int. J. Adhes. Adhes. 29, 23–31. https://doi.org/10.1016/j.ijadhadh.2008.01.001.

Ramaswamy, K., O'Higgins, R.M., Kadiyala, A.K., McCarthy, M.A., McCarthy, C.T., 2020. Evaluation of grit-blasting as a pre-treatment for carbon-fibre thermoplastic composite to aluminium bonded joints tested at static and dynamic loading rates. Compos. B Eng. 185, 107765. https://doi.org/10.1016/j.compositesb.2020.107765.

Ravi-Kumar, S., Lies, B., Zhang, X., Lyu, H., Qin, H., 2019. Laser ablation of polymers: a review. Polym. Int. 34, 316–327. https://doi.org/10.1002/pi.5834.

Rudawska, A., Jacniacka, E., 2009. Analysis for determining surface free energy uncertainty by the Owen-Wendt method. Int. J. Adhes. Adhes. 29, 451–457. https://doi.org/10.1016/j.ijadhadh.2008.09.008.

Schweizer, M., Meinhard, D., Ruck, S., Riegel, H., Knoblauch, V., 2017. Adhesive bonding of CFRP: a comparison of different surface pre-treatment strategies and their effect on the bonding shear strength. J. Adhes. Sci. Technol. 31, 2581–2591. https://doi.org/10.1080/01694243.2017.1310695.

Tao, R., Alfano, M., Lubineau, G., 2018. Laser-based surface patterning of composite plates for improved secondary adhesive bonding. Compos. Part A Appl. Sci. Manuf. 109, 84–94. https://doi.org/10.1016/j.compositesa.2018.02.041.